

This is a repository copy of *Correlation between spin transport signal and Heusler/semiconductor interface quality in lateral spin-valve devices*.

White Rose Research Online URL for this paper:

<https://eprints.whiterose.ac.uk/136059/>

Version: Accepted Version

Article:

Lazarov, Vlado orcid.org/0000-0002-4314-6865, Kuerbanjiang, Balati orcid.org/0000-0001-6446-8209, Ghasemi, Arsham et al. (8 more authors) (2018) Correlation between spin transport signal and Heusler/semiconductor interface quality in lateral spin-valve devices. Physical Review B. 115304. ISSN 2469-9969

<https://doi.org/10.1103/PhysRevB.98.115304>

Reuse

Items deposited in White Rose Research Online are protected by copyright, with all rights reserved unless indicated otherwise. They may be downloaded and/or printed for private study, or other acts as permitted by national copyright laws. The publisher or other rights holders may allow further reproduction and re-use of the full text version. This is indicated by the licence information on the White Rose Research Online record for the item.

Takedown

If you consider content in White Rose Research Online to be in breach of UK law, please notify us by emailing eprints@whiterose.ac.uk including the URL of the record and the reason for the withdrawal request.

Correlation between spin transport signal and Heusler/semiconductor interface quality in lateral spin-valve devices

B. Kuerbanjiang,¹ Y. Fujita,² M. Yamada,² S. Yamada,^{2,3} A. M. Sanchez,⁴ P. J. Hasnip,¹ A. Ghasemi,¹ D. Kepaptsoglou,⁵ G. Bell,⁴ K. Sawano,⁶ K. Hamaya^{2,3} and V. K. Lazarov¹

¹ *Department of Physics, University of York, York YO10 5DD, United Kingdom.*

² *Graduate School of Engineering Science, Osaka University,
1-3 Machikaneyama, Toyonaka 560-8531, Japan.*

³ *Center for Spintronics Research Network, Osaka University,
1-3 Machikaneyama, Toyonaka 560-8531, Japan.*

⁴ *Department of Physics, University of Warwick, Coventry CV4 7AL, United Kingdom.*

⁵ *SuperSTEM laboratory, SciTeck Daresbury Campus, Daresbury WA4 4AD, United Kingdom. and*

⁶ *Advanced Research Laboratories, Tokyo City University, 8-15-1 Todoroki, Tokyo 158-0082, Japan.*

(Dated: August 1, 2018)

We show a direct evidence for the impact of Heusler/semiconductor interfaces atomic structure on the spin transport signals in semiconductor-based lateral spin-valve (LSV) devices. Based on atomic scale Z contrast scanning transmission electron microscopy and energy dispersive x-ray spectroscopy we show that atomic order/disorder of $\text{Co}_2\text{FeAl}_{0.5}\text{Si}_{0.5}$ (CFAS)/ n -Ge LSV devices is critical for the spin injection in Ge. By conducting a post annealing of the LSV devices, we find 90% decrease in the spin signal while there is no difference in the electrical properties of the CFAS/ n -Ge contacts and in the spin diffusion length of the n -Ge layer. We show that the reduction in the spin signals after annealing is attributed to the presence of intermixing phases at the Heusler/semiconductor interface. First principles calculations show how that intermixed interface region has drastically reduced spin polarisation at the Fermi level, which is the main cause for the significant decrease of the spin signal in the annealed devices above 300 °C.

Semiconductor (SC)-based spintronics has been explored for novel information storage and logic devices utilizing the spin angular momentum¹⁻⁷. Recent works have clarified some important parameters such as spin lifetime and spin diffusion length in SCs by using four-terminal nonlocal measurements⁸⁻¹⁰, which are the most reliable methods, in lateral spin-valve (LSV) devices with GaAs^{4,11-13}, Si¹⁴⁻¹⁶, and Ge channels¹⁷⁻²¹.

In general, highly efficient electrical creation and detection of spin currents in SCs are particularly important for the fundamental concepts of spin transistors^{22,23}. For n -type GaAs, the spin injection and detection in LSVs has been reported, emphasising the role of the interface^{4,12,13}. However, there is almost no discussion about the direct comparison between the magnitude of the nonlocal spin signals and the atomic structural ordering of the Heusler/SC interfaces. Furthermore, it is of crucial importance knowing how annealing, a common procedure in Heusler based spin-devices undertaken for improving the structural and chemical ordering of the deposited films, will affect spin polarization and overall magnetic/electronic properties of Heusler/SC based devices. Recently, for n -type Ge, we have pioneered and demonstrated the spin injection/detection techniques with ferromagnetic Heusler-alloy/Ge heterointerfaces^{20,24,25}, which allow us to address the relevant interface phenomena using the LSVs with the Heusler-alloy/Ge contacts.

In this work, the nonlocal spin signals are examined for LSVs with as-prepared and annealed Heusler-alloy/Ge contacts. Nonlocal spin signals are strikingly decreased down to less than a tenth after annealing at 300 °C. It

should be noted that between as-prepared and annealed devices there is no difference in the electrical properties of the Heusler-alloy/ n -Ge contacts and spin diffusion length of the n -Ge layer. Based on high angle annular dark field (HAADF) scanning transmission electron microscopy (STEM) imaging and energy dispersive X-ray spectroscopy (EDS) analysis, we show that the reduction in the spin signals after annealing is attributed to the presence of intermixing phases at the Heusler-alloy/Ge interfaces. This means that the loss of the interface atomic and chemical abruptness affects significantly the amplitude of the detected spin signals in the semiconductor spintronic devices. We compare and discuss intermixing of Heusler/Ge interface between as-prepared and annealed LSVs.

A schematic of the used LSV with Heusler-alloy/ n -Ge contacts and measurement scheme for four-terminal non-local magnetoresistance are shown in Fig. 1(a). Here we used $\text{Co}_2\text{FeAl}_{0.5}\text{Si}_{0.5}$ (CFAS) as a spin injector and a detector^{24,25}. To promote the tunneling conduction for spin injection and detection, a P δ -doped Ge layer with an ultra-thin Si insertion was grown at CFAS/ n -Ge interfaces. The detailed procedures of the crystal growth of CFAS films and n -Ge spin-transport layers were shown elsewhere^{24,26,27}. The carrier concentration (n) in the n -Ge layer was $n \sim 8.0 \times 10^{18} \text{ cm}^{-3}$, estimated from the Hall-effect measurements. The two different CFAS/ n -Ge contacts with $0.4 \times 5.0 \mu\text{m}^2$ and $1.0 \times 5.0 \mu\text{m}^2$ in size were fabricated by conventional electron-beam lithography and Ar-ion milling. The centre-to-centre distances between the CFAS/ n^+ -Ge contacts were designed to be $1.1 \mu\text{m}$. Post annealing for LSVs was conducted at 150,

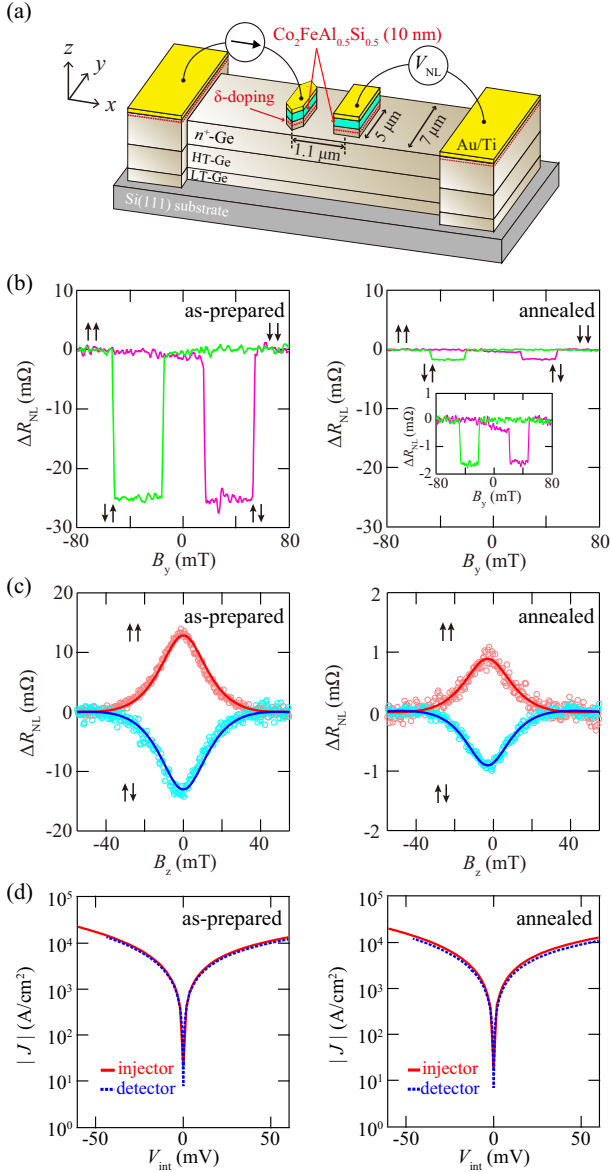


FIG. 1. (Colour online) (a) Schematic illustration of the fabricated CFAS/*n*-Ge based LSV. (b) Nonlocal magnetoresistance curve and (c) Hanle curves at 8 K for as-prepared and annealed LSVs. (d) $J - V$ characteristics for the CFAS/*n*-Ge contacts in as-prepared and annealed LSVs.

200, 250, 300 and 400 °C for 10 min under N₂ gas at ambient pressure. To detect spin transport in *n*-Ge, non-local magnetoresistance ($\Delta R_{NL} = \Delta V_{NL}/I$) curves were measured by applying in-plane or out of plane magnetic fields (B_y or B_z).

Cross-sectional transmission electron microscopy samples were prepared by focused-ion-beam (FIB) technique and by conventional methods that include mechanical thinning and Ar ion milling²⁸. Atomic-level structural studies were performed by HAADF STEM imaging on a Nion UltraSTEM 100 microscope, operated at 100 kV, with a convergence angle of 30 mrad; at these optical con-

ditions the electron probe size is determined to be 0.9 Å; the inner detector angle for HAADF STEM imaging was 76 mrad. Further atomic-level STEM analysis was performed using ARM200F microscope with probe and image aberration CEOS correctors operating at 300 kV. Annular Dark Field images were obtained with a JEOL annular field detector with an inner angle of 70 mrad; fine imaging probe of ~23 pA and convergence semi-angle of ~22 mrad. EDS analysis was performed with probe currents of approximately 200 pA and collected with a windowless Oxford Instruments X-Max Silicon Drift Detector with area of 100 mm². Density functional theory (DFT) calculations were performed with the CASTEP code²⁹. The PBE+U exchange correlation functional was used, and a Hubbard-U term set to 2.1 eV for both d-block elements Co and Fe. This value for the Hubbard-U term has previously been shown to open up the minority band-gap, approximately correcting for the delocalising effect of self-interaction with PBE alone³⁰. The plane wave cut-off energy was set to 600 eV, while the Brillouin zone was sampled using a Monkhorst-Pack grid with a k -point sampling spacing of $0.035 \, 2\pi \text{Å}^{-1}$.

Fig. 1(b) shows a comparison of the nonlocal magnetoresistance curves at 8 K between as-prepared and annealed LSVs, where the annealing temperature is 300 °C. For the annealed LSV, the spin signal is degraded down to ~1.5 mΩ whereas a spin signal of ~25 mΩ is obtained for the as-prepared LSV. If the annealing temperature was risen up to 400 °C, we could not see such spin signals even at 8 K (not shown here). Also, the annealing below 250 °C did not affect the value of the spin signals. Thus, we can infer that the post annealing above 300 °C affects the detection of spin transport in CFAS/*n*-Ge-based LSVs.

In Fig. 1(c) we also measure the nonlocal Hanle effect under parallel and anti-parallel magnetization configurations to record ΔR_{NL} as a function of B_z . For both LSVs, evident spin precession curves (Hanle curves) can be seen. Using the Hanle curves, we can roughly extract τ_{Ge} and the diffusion constant (D) values in *n*-Ge. According to the previous works^{4,9}, the nonlocal Hanle curves are expressed as the following one dimensional spin drift diffusion model,

$$\Delta R_{NL}(B_z) = \pm A \int_0^\infty \phi(t) \cos(\omega_L t) \exp\left(-\frac{t}{\tau_{Ge}}\right) dt, \quad (1)$$

where $A = \frac{P_{inj} P_{det} \rho_{Ge} D}{S}$, $\phi(t) = \frac{1}{\sqrt{4\pi Dt}} \exp\left(-\frac{L^2}{4Dt}\right)$, $\omega_L (= g\mu_B B_z/\hbar)$ is the Larmor frequency, g is the electron g -factor ($g = 1.56$) in Ge³¹, and μ_B is the Bohr magneton. Here, P_{inj} and P_{det} are the spin polarization of the electrons in *n*-Ge, created by the spin injector and detector, respectively, ρ_{Ge} is the resistivity ($1.74 \text{ m}\Omega\text{cm} \leq \rho_{Ge} \leq 1.83 \text{ m}\Omega\text{cm}$), S is the cross section ($S = 0.49 \, \mu\text{m}^2$) of the *n*⁺-Ge layer used here, and L is the center-to-center distance between the spin injector and detector ($L = 1.1 \, \mu\text{m}$). Here we have confirmed that there is no change in $J - V$ characteristics for the

TABLE I. Comparison of the extracted parameters from Hanle curves at 8 K for as-prepared and annealed LSVs.

	as-prepared LSV	annealed LSV
τ_{Ge} (ns)	0.46 ± 0.002	0.48 ± 0.05
D (cm^2/s)	10.34 ± 0.02	9.78 ± 0.27
λ_{Ge} (μm)	0.69	0.68

CFAS/ n -Ge contacts in as-prepared and annealed LSVs, as shown in Fig. 1(d), and no influence of the contact-induced spin relaxation on the Hanle analysis³². **Considering the electrical property in Fig. 1(d), we can judge that the tunneling mechanism did not change to the two-step tunneling through the interface states. Thus, we do not have to consider the two step model for spin injection into a semiconductor through interface states³³.**

The solid curves presented in Fig. 1(c) indicate the results fitted to Eq. (1). From these analyses, the extracted τ_{Ge} and D are summarized in Table I, together with the calculated spin diffusion length ($\lambda_{\text{Ge}} = \sqrt{D\tau_{\text{Ge}}}$). For both LSVs, all the parameters are nearly the same, meaning that the post annealing at 300 °C did not affect τ_{Ge} , D , and λ_{Ge} . In addition these values are consistent with the experimental data previously reported^{19,24,25} and the expected values from the recent theoretical studies for heavily doped n -Ge^{34,35}. For these reasons, we deduce that the magnitude of the nonlocal spin transport signals is significantly influenced by factors different than the spin lifetime and the spin diffusion length in the spin transport layers. From Eq. (1) and these parameters in Table I, we can also estimate the spin polarization ($\sqrt{P_{\text{inj}}P_{\text{det}}}$) of as-prepared and annealed LSVs to be ~ 0.067 and ~ 0.022 , respectively, at 8 K. After the annealing, the $\sqrt{P_{\text{inj}}P_{\text{det}}}$ is reduced down to one-third in our LSVs.

Next we explore the structural properties of CFAS/ n -Ge interfaces in order to find out the correlation between the structure and reduction of the spin polarization in the interface region. We focus on the presence of atomic disorder or secondary phases formation as a potential source for the strong reduction in the $\sqrt{P_{\text{inj}}P_{\text{det}}}$ from ~ 0.067 to ~ 0.022 . For cross-sectional HAADF-STEM analysis we selected two representative LSV devices, the device with best performance (as-prepared) and the device that has drastically reduced spin signal (annealed at 300 °C). Fig. 2(a) is a cross-sectional overview of the fabricated LSV device, clearly showing the uniformity and morphology of the deposited device layers, including the Ti and Au device contacts. Fig. 2(b) is atomic resolution HAADF STEM images of the CFAS/ n^+ -Ge interface from the region outlined in Fig. 2(a). Single crystal $B2$ ordering of the CFAS is clearly seen (see also Fig. S1(a) in the Supplementary Material³⁶), as well as few atomic layers (~ 3 Å) of δ -doped P + Si insertion. The different crystallographic structure of Ge and CFAS shows the structural abruptness of the interface, and epitaxial relationship between the layers, previously stud-

ied in details when CFAS is directly deposited on single crystal Ge(111) substrates^{37,38}. We also note a presence of n^+ -Ge(111) atomic step terraces at the interface. In contrast to the as-prepared device, the annealed device show distinctively different interface and film structure. Fig. 2(c) shows interface region of the CFAS film and n^+ -Ge layer. First to notice is the increased CFAS layer thickness (in comparison to the as-prepared specimen) indicating an interface mixing, i.e. strong interdiffusion at the CFAS/Ge interface. While the as-prepared specimen has a predominant $B2$ ordered single crystalline CFAS phase, the annealed specimen shows grain formation with different texture (see Fig. S1(b)-(d) in the supplementary material³⁶). The Z contrast variation within 5 nm of the Heusler film interface region indicates non-homogeneous chemical elemental distribution in this region. We performed EDS line profile across the interface regions to elucidate elemental distribution across the interface region.

Fig. 3 shows two representative EDS elemental line profiles across the CFAS/ n^+ -Ge interface of as-prepared and annealed LSV devices. Simultaneous HAADF and EDS acquisition show that in both as-prepared and annealed devices intermixing take place, and it is larger in the annealed device. As Fe/Co and Al/Si diffuse in Ge channel, Ge is outdiffusing in CFAS electrode. The extend of the intermixed region is ~ 3 nm in as-prepared device and ~ 5 nm in the annealed (at 300 °C) device. These findings are distinctively different from the case where the interfaces created between a CFAS thin film and a Ge(111) single crystal substrate, which are structurally and chemically abrupt, only with small selective atomic plane outdiffusion of Ge³⁷. Moreover, a mutual intermixing occurs at much higher annealing temperatures, above 450 °C³⁸. These differences are suggesting that there is a further room for optimising spin-injection by improving the Heusler/SC interface quality.

The structural changes induced by annealing were also observed by magnetometry (performed by vibrating sample magnetometer) on device structures before the fabrication. There is a 16 % decrease of saturation magnetization (M_s) and a two times increase of the coercivity (H_c) after annealing the device structure at 300 °C as shown in Fig. S2 in the Supplementary Material³⁶. This is a further proof that Ge in the intermixed region substitutes magnetic Co and Fe, as the substitution of Al and Si which bring only negligible change in the overall specimen magnetization³⁷. The increase of coercivity is very likely driven by the grain boundaries formation in the CFAS film in the annealed specimens as well as formation of mixed CFAS+Ge regions which can act as pinning sites. Furthermore, the normalized M_s of as-prepared device structure compared to the CFAS film grown on Ge(111) single crystal substrate, shows a decrease of 26 %.

The chemical disorder created at the interface due to interdiffusion will change the spin polarization of the CFAS electrode in the interface region, since the spin polarization is critically dependent of the chemical or-

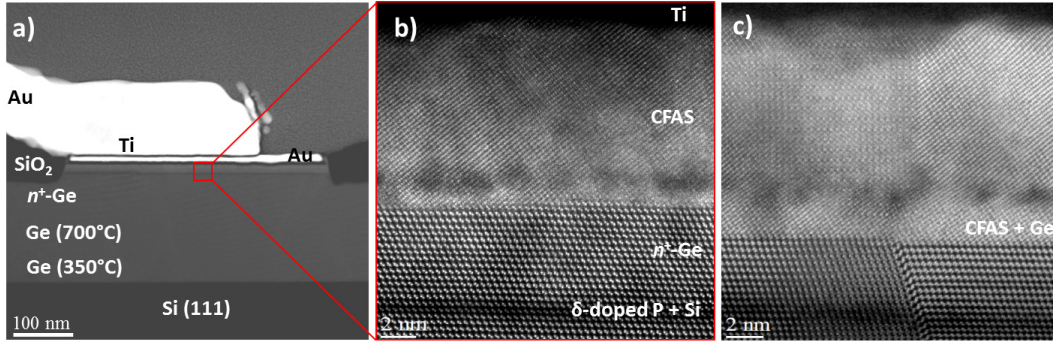


FIG. 2. (Colour online) (a) Low mag HAADF STEM image of the LSV device structure, showing an overall geometry of the fabricated device. The structural ordering of the CFAS/ n^+ -Ge interface region of the as-prepared (b) and the annealed samples (c) viewed along $[\bar{1}10]$ zone axis show drastic change after heat treatment. Annealed sample has multiple crystalline CFAS film domains.

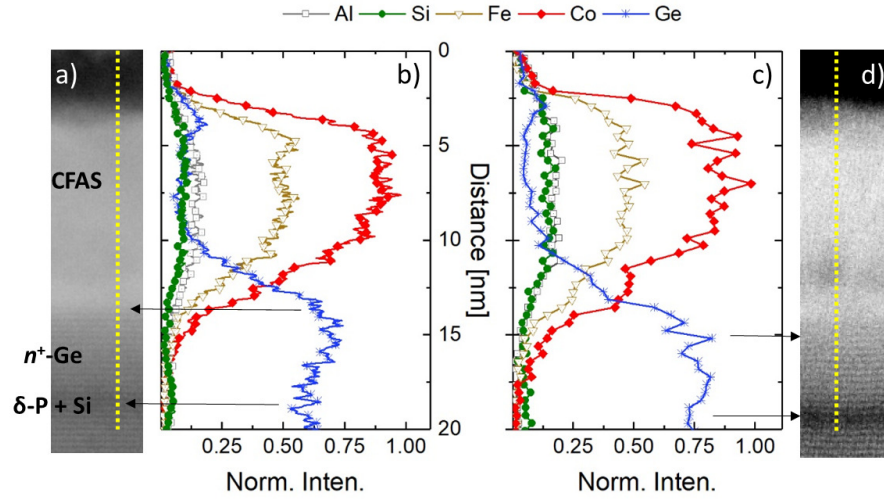


FIG. 3. (Colour online) (a) A HAADF STEM image of CFAS/ n^+ -Ge region, an EDS line scan of the as-prepared sample (b) is collected along the yellow dashed line. [(c),(d)] EDS line scan of the similar area of the annealed sample for comparison. Arrows are guides for the eye.

dering in the Heusler electrode³⁹. In order to assess the spin polarization and the magnetic moment of the mixed interface region, we consider the effect of Ge substitution of the CFAS lattice by performing DFT calculations on a supercell of $2 \times 2 \times 2$ conventional cells for various amounts of Ge substitution. The results of a few representative configurations are presented in Table II, and extensive results presented in the supplementary materials in Table S1³⁶. When Ge substitutes Al/Si, the spin polarization does not change. However, the progressive substitution of Fe and Co can drastically reduce the spin polarization and the magnetic moment of the CFAS electrode in the interface region. **This is due to decreased hybridisation of the Co d orbitals, which results in their delocalisation at the Fermi level, and consequent closing of the minority band gap (FIG. S3).** We note that even small concentrations of the Ge substitution of Co can kill the spin polarisation and that above $\sim 15\%$ substitution the overall spin polarisation of CFAS becomes negative at

the Fermi level (FIG. S4). The detailed results presented in Table II and Table S1 in the Supplementary Material³⁶ directly correlate with the observed decrease of the overall magnetization (M) of the Heusler electrode, as well as the significant decrease of the magnitude of the spin signal observed in nonlocal device measurements presented above.

In summary, we demonstrate direct correlation between the interface structure and spin signal magnitude in lateral spin valve devices. The nonlocal measurements show significant drop of the magnitude of the spin signal when devices are annealed above 300°C . This decrease of the spin signal is due to the formation of intermixed interface region between CFAS and Ge. The mutual diffusion of Ge and most notable, Co from CFAS create an interface region of ~ 5 nm, which has gradual decrease in the electrode spin polarization that ultimately affect the magnitude of the spin signal detected. Moreover, the structural studies of the devices in com-

TABLE II. First-principles calculation results showing the dependence of the magnetic moment M and polarisation P as a function of the concentration of Ge substituting atoms in CFAS. $n(\text{Si})$, $n(\text{Al})$, $n(\text{Fe})$, $n(\text{Co})$ and $n(\text{Ge})$ stand for the number of Si, Al, Fe, Co and Ge, respectively, in a considered configuration. The first row represents bulk CFAS where the unit cell has 16 atoms. Note that using a general X_2YZ formula for full Heusler alloys, X represents the sublattice of Co, Y sublattice of Fe, and Z the sublattice of Al/Si.

Label	$n(\text{Si})$	$n(\text{Al})$	$n(\text{Fe})$	$n(\text{Co})$	$n(\text{Ge})$	M [$\mu_{\text{B}}/\text{u.c.}$]	$P[\%]$
Bulk	16	16	32	64	0	176.0	100
Z8	8	16	32	64	8	176.1	100
Z16	0	16	32	64	16	176.4	100
Z24	16	8	32	64	24	184.0	100
Z32	16	0	32	64	32	192.0	100
Y8	16	16	24	64	8	144.4	99
Y16	16	16	16	64	16	114.0	56
Y24	16	16	8	64	24	83.7	39
Y32	16	16	0	64	32	52.3	45
X8	16	16	32	56	8	173.6	20
X16	16	16	32	48	16	150.1	-16
X24	16	16	32	40	24	122.0	-15
X32	16	16	32	32	32	94.6	-21.5

ACKNOWLEDGEMENTS

This work was partly supported by a Grant-in-Aid for Scientific Research (A) (No. 16H02333) and (S) (No. 17H06120) from the Japan Society for the Promotion of Science (JSPS), and a Grant-in-Aid for Scientific Research on Innovative Areas ‘Nano Spin Conversion Science’ (No. 26103003) from the Ministry of Education, Culture, Sports, Science and Technology (MEXT). Part of the work was funded by the Engineering and Physical Sciences Research Council (EPSRC) through grants EP/K03278X/1 and EP/K032852/1. The SuperSTEM Laboratory is the U.K. National Facility for Aberration-Corrected STEM, supported by the EPSRC. The authors are grateful for computational support from the UK national High Performance Computing service ARCHER.

- ¹ I. Žutić, J. Fabian, and S. D. Sarma, Spintronics: Fundamentals and applications, *Rev. Mod. Phys.* **76**, 323 (2004).
- ² H. Dery, P. Dalal, L. Cywiński, and L. J. Sham, Spin-based logic in semiconductors for reconfigurable large-scale circuits, *Nature (London)* **447**, 573 (2007).
- ³ M. Tanaka and S. Sugahara, MOS-Based Spin Devices for Reconfigurable Logic, *IEEE Trans. Electron Devices* **54**, 961 (2007).
- ⁴ X. Lou, C. Adelman, S. A. Crooker, E. S. Garlid, J. Zhang, K. S. M. Reddy, S. D. Flexner, C. J. Palmström, and P. A. Crowell, Electrical detection of spin transport in lateral ferromagnet-semiconductor devices, *Nat. Phys.* **3**, 197 (2007).
- ⁵ I. Appelbaum, B. Huang, and D. J. Monsma, Electronic measurement and control of spin transport in silicon, *Nature* **447**, 295 (2007).
- ⁶ B. T. Jonker, G. Kioussoglou, A. T. Hanbicki, C. H. Li, and P. E. Thompson, Electrical spin-injection into silicon from a ferromagnetic metal/tunnel barrier contact, *Nat. Phys.* **3**, 542 (2007).
- ⁷ R. Jansen, Silicon spintronics, *Nat. Mater.* **11**, 400 (2012).
- ⁸ M. Johnson and R. H. Silsbee, Interfacial charge-spin coupling: Injection and detection of spin magnetization in metals, *Phys. Rev. Lett.* **55**, 1790 (1985).
- ⁹ F. J. Jedema, H. B. Heersche, A. T. Filip, J. J. A. Baselmans, and B. J. van Wees, Electrical detection of spin precession in a metallic mesoscopic spin valve, *Nature (London)* **416**, 713 (2002).
- ¹⁰ T. Kimura and Y. Otani, Spin transport in lateral ferromagnetic/nonmagnetic hybrid structures, *J. Phys. Condens. Matter.* **19**, 165216 (2007).
- ¹¹ M. Ciorga, A. Einwanger, U. Wurstbauer, D. Schuh, W. Wegscheider, and D. Weiss, Electrical spin injection and detection in lateral all-semiconductor devices, *Phys. Rev. B* **79**, 165321 (2009).
- ¹² G. Salis, S. F. Alvarado, and A. Fuhrer, Spin-injection spectra of CoFe/GaAs contacts: Dependence on Fe concentration, interface, and annealing conditions, *Phys. Rev. B* **84**, 041307(R) (2011).
- ¹³ T. A. Peterson, S. J. Patel, C. C. Geppert, K. D. Christie, A. Rath, D. Pennachio, M. E. Flatté, P. M. Voyles, C. J. Palmström, and P. A. Crowell, Spin injection and detection up to room temperature in Heusler alloy/ n -GaAs spin valves, *Phys. Rev. B* **94**, 235309 (2016).
- ¹⁴ O. M. J. van’t Erve, A. T. Hanbicki, M. Holub, C. H. Li, C. Awo-Affouda, P. E. Thompson, and B. T. Jonker, Electrical injection and detection of spin-polarized carriers in silicon in a lateral transport geometry, *Appl. Phys. Lett.* **91**, 212109 (2007).
- ¹⁵ T. Suzuki, T. Sasaki, T. Oikawa, M. Shiraishi, Y. Suzuki, and K. Noguchi, Room-Temperature Electron Spin Transport in a Highly Doped Si Channel, *Appl. Phys. Express* **4**, 023003 (2011).
- ¹⁶ M. Ishikawa, T. Oka, Y. Fujita, H. Sugiyama, Y. Saito, and K. Hamaya, Spin relaxation through lateral spin transport in heavily doped n -type silicon, *Phys. Rev. B* **95**, 115302 (2017).
- ¹⁷ Y. Zhou, W. Han, L.-T. Chang, F. Xiu, M. Wang, M. Oehme, I. A. Fischer, J. Schulze, R. K. Kawakami, and K. L. Wang, Electrical spin injection and transport in germanium, *Phys. Rev. B* **84**, 125323 (2011).

- ¹⁸ K. Kasahara, Y. Fujita, S. Yamada, K. Sawano, M. Miyao and K. Hamaya, Greatly enhanced generation efficiency of pure spin currents in Ge using Heusler compound Co_2FeSi electrodes, *Appl. Phys. Express* **7**, 033002 (2014).
- ¹⁹ Y. Fujita, M. Yamada, S. Yamada, T. Kanashima, K. Sawano, and K. Hamaya, Temperature-independent spin relaxation in heavily doped n -type germanium, *Phys. Rev. B* **94**, 245302 (2016).
- ²⁰ M. Yamada, M. Tsukahara, Y. Fujita, T. Naito, S. Yamada, K. Sawano, and K. Hamaya, Room-temperature spin transport in n -Ge probed by four-terminal nonlocal measurements, *Appl. Phys. Express* **10**, 093001 (2017).
- ²¹ F. Rortais, C. Vergnaud, A. Marty, L. Vila, J.-P. Attané, J. Wdziez, C. Zuchetti, F. Bottegioni, H. Jaffrès, J.-M. George, and M. Jamet, Non-local electrical spin injection and detection in germanium at room temperature, *Appl. Phys. Lett.* **111**, 182401 (2017).
- ²² S. Datta and D. Das, Electronic analog of the electro-optic modulator, *Appl. Phys. Lett.* **56**, 665 (1990).
- ²³ P. Chuang, S.-C. Ho, L. W. Smith, F. Sfigakis, M. Pepper, C.-H. Chen, J.-C. Fan, J. P. Griffiths, I. Farrer, H. E. Beere, G. A. C. Jones, D. A. Ritchie, and T.-M. Chen, All-electric all-semiconductor spin field-effect transistors, *Nat. Nanotechnol.* **10**, 35 (2015).
- ²⁴ Y. Fujita, M. Yamada, M. Tsukahara, T. Oka, S. Yamada, T. Kanashima, K. Sawano, and K. Hamaya, Spin transport and relaxation up to 250 K in heavily doped n -type Ge detected using $\text{Co}_2\text{FeAl}_{0.5}\text{Si}_{0.5}$ electrodes, *Phys. Rev. Applied* **8**, 014007 (2017).
- ²⁵ M. Yamada, Y. Fujita, M. Tsukahara, S. Yamada, K. Sawano, and K. Hamaya, Large impact of impurity concentration on spin transport in degenerate n -Ge, *Phys. Rev. B* **95**, 161304(R) (2017).
- ²⁶ S. Yamada, K. Tanikawa, S. Oki, M. Kawano, M. Miyao and K. Hamaya, Improvement of magnetic and structural stabilities in high-quality $\text{Co}_2\text{FeSi}_{1-x}\text{Al}_x/\text{Si}$ heterointerfaces, *Appl. Phys. Lett.* **105**, 071601 (2014).
- ²⁷ K. Tanikawa, S. Oki, S. Yamada, M. Kawano, M. Miyao, and K. Hamaya, High-quality $\text{Co}_2\text{FeSi}_{0.5}\text{Al}_{0.5}/\text{Si}$ heterostructures for spin injection in silicon spintronic devices *Thin Solid Films* **557**, 390 (2014).
- ²⁸ B. Kuerbanjiang, Z. Nedelkoski, D. Kepaptsoglou, A. Ghasemi, S. E. Glover, S. Yamada, T. Saerbeck, Q. M. Ramasse, P. J. Hasnip, T. P. A. Hase, G. R. Bell, K. Hamaya, A. Hirohata, and V. K. Lazarov, The role of chemical structure on the magnetic and electronic properties of $\text{Co}_2\text{FeAl}_{0.5}\text{Si}_{0.5}/\text{Si}(111)$ interface, *Appl. Phys. Lett.* **108**, 172412 (2016).
- ²⁹ S. J. Clark, M. D. Segall, C. J. Pickard, P. J. Hasnip, M. I. J. Probert, K. Refson, and M. C. Payne, First principles methods using CASTEP, *Z. Kristallogr. Cryst. Mater.* **220**, 567 (2005).
- ³⁰ P. J. Hasnip, J. H. Smith, and V. K. Lazarov, *Ab initio* studies of disorder in the full Heusler alloy $\text{Co}_2\text{Fe}_x\text{Mn}_{1-x}\text{Si}$, *J. Appl. Phys.* **113**, 17B106 (2013).
- ³¹ R. Vrijen, E. Yablonovitch, K. Wang, H. W. Jiang, A. Balandin, V. Roychowdhury, T. Mor, and D. Divincenzo, Electron-spin-resonance transistors for quantum computing in silicon-germanium heterostructures, *Phys. Rev. A* **62**, 012306 (2000).
- ³² L. O'Brien, D. Spivak, N. Krueger, T. A. Peterson, M. J. Erickson, B. Bolon, C. C. Geppert, C. Leighton, and P. A. Crowell, Observation and modeling of ferromagnetic contact-induced spin relaxation in Hanle spin precession measurements, *Phys. Rev. B* **94**, 094431 (2016).
- ³³ M. Tran, H. Jaffrès, C. Deranlot, J.-M. George, A. Fert, A. Miard, and A. Lemaître, Enhancement of the spin accumulation at the interface between a spin-polarized tunnel junction and a semiconductor, *Phys. Rev. Lett.* **102**, 036601 (2009).
- ³⁴ P. Li, Y. Song, and H. Dery, Intrinsic spin lifetime of conduction electrons in germanium, *Phys. Rev. B* **86**, 085202 (2012).
- ³⁵ Y. Song, O. Chalaev, and H. Dery, Donor-driven spin relaxation in multivalley semiconductors, *Phys. Rev. Lett.* **113**, 167201 (2014).
- ³⁶ (Link to the Supplementary file, will be added later).
- ³⁷ Z. Nedelkoski, B. Kuerbanjiang, S. E. Glover, A. Sanchez, D. Kepaptsoglou, A. Ghasemi, C. W. Burrows, S. Yamada, K. Hamaya, Q. Ramasse, P. Hasnip, T. Hase, G. Bell, A. Hirohata, and V. Lazarov, Realisation of magnetically and atomically abrupt halfmetal/semiconductor interfaces: $\text{Co}_2\text{FeAl}_{0.5}\text{Si}_{0.5}/\text{Ge}(111)$, *Sci. Rep.* **6**, 37282 (2016).
- ³⁸ B. Kuerbanjiang, C. Love, D. Kepaptsoglou, Z. Nedelkoski, S. Yamada, A. Ghasemi, Q. M. Ramasse, K. Hamaya, S. A. Cavill, and V. K. Lazarov, Effect of annealing on the structure and magnetic properties of $\text{Co}_2\text{FeAl}_{0.5}\text{Si}_{0.5}$ thin films on Ge (111), *J. Alloys Compd.* **748**, 323-327 (2018).
- ³⁹ P. J. Hasnip, C. H. Loach, J. H. Smith, M. I. J. Probert, D. Gilks, J. Sizeland, L. Lari, J. Sagar, K. Yoshida, M. Oogane, A. Hirohata, and V. K. Lazarov, The effect of cobalt-sublattice disorder on spin polarisation in $\text{Co}_2\text{Fe}_x\text{Mn}_{1-x}\text{Si}$ Heusler alloys, *Materials*, **7**, 1473-1482 (2014).